Deep Brain Drug-delivery Control using Vagus Nerve Communications

Michael Donohoe[a,*], Brendan Jennings[a], Sasitharan Balasubramaniam[1]

[a]*Telecommunications Software & Systems Group (TSSG), Waterford Institute of Technology, Ireland*

Abstract

Vagus nerve stimulation (VNS) uses electrical impulses applied at the neck in order to mitigate the effects of, for example, epileptic seizures. We propose using VNS to provide data pulses to communicate with a drug-delivery system embedded near the brainstem. We model the generation of a vagus nerve compound action potential (CAP), calculating the signal attenuation and the resulting transmission range. The metabolic cost of CAP transmission in terms of the use of adenosine triphosphate (ATP) is also calculated. The channel capacity for on-off keying (OOK) is computed from the CAP characteristics, the neural refractory period and the level of background neural noise. The resulting low bit-rate, unidirectional asynchronous transmission system is analysed for the use of different methods of forward error correction (FEC) to improve bit-error rate (BER). We show a proposed data packet structure that could deliver instructions to an embedded drug-delivery system with multiple addressable drug reservoirs. We also analyse the scope for powering the drug-delivery system with energy harvested from cerebrospinal glucose.

Keywords: `Vagus Nerve, Compound Action Potential, Neural Transmission, Forward Error Correction`

1. Introduction

Communicating with powered implants embedded in the human body, such as cardiac pacemakers or defibrillators, is an increasingly important part of medical treatment. Wireless communications systems provide a bidirectional flexible link over short ranges [1], but place power requirements of hundreds of microwatts on an implant [2]. Apart from the power requirements, the transmission of commands from an external wireless electromagnetic *(EM)* module to an implanted device does create security implications and may be subject to hacking [3]. An alternative method is to use the peripheral or cranial nervous system in the body to transport data commands from a transmitter at one point on a nerve to an embedded receiver at another point. The use of neural communications is part of wider research into implanted devices at the micro and nano level [4] where restrictions in antenna size will limit the use of EM systems.

Data communications using *action potentials (AP)* along a single neuronal axon is proposed by Parcerisa-Giné and Akyildiz [5] as an option for providing a physical link between embedded micro devices. Channel models for communications using neural spikes (APs) and neurotransmitters between hippocampal neurons have been developed by Malak and Akan [6], Ramezani and Akan [7] and Veletić et al [8]. Data communications through the single median giant axon of the earthworm was modelled by Abbasi et al [9] who calculated a data throughput based on four different stimulus frequencies, with each frequency representing two bits of information. A neuron channel model using a sub-threshold (non-spiking) stimulus was proposed by Khodaei and Pierobon [10] [11], though sub-threshold impulses have a very short range along an axon [12]. Single neurons are, however, difficult to access and the placement of transmitters and receivers would be particularly challenging. Consequently, it could be more practical to examine the collective stimulus of multiple neurons forming a *compound action potential (CAP)* to provide a neural data pulse.

There is ongoing research into the use of *vagus nerve stimulation (VNS)* for the treatment of epileptic seizures [13], depression, heart failure [14], arthritis [15] and Crohn's disease. At present a VNS system relies on human

*Corresponding Author

Email addresses: `mdonohoe@tssg.org` (Michael Donohoe), `bjennings@tssg.org` (Brendan Jennings), `sasib@tssg.org` (Sasitharan Balasubramaniam)

intervention by the physician and patient to programme the duration and intensity of the stimulus pulses. A more flexible biofeedback system is proposed by Ward et al [16] using the degree of measured nerve activation to control stimulus delivery and provide a personalised stimulus profile. Non-stimulus based therapies include drug-delivery to the brain, although the protective *blood-brain barrier (BBB)* presents a challenge for the absorption of drugs [17] to treat, for example, cancer tumours. A drug-delivery system for treating epilepsy is described by Salam et al [18] with embedded electrodes to detect seizures and a micromechanical pump to deliver the drug from a refillable reservoir located under the scalp. A neural probe with an electrophoretic microfluidic ion pump is proposed by Proctor et al [19] to deliver variable doses of a single drug across an ion-exchange membrane. Another release mechanism is *electrothermal membrane activation*, first proposed by Santini et al [20], where a metallic membrane covers a drug reservoir. An electrical current ruptures the membrane by heating and the drug reservoir releases its contents. Either of these delivery systems could be controlled by a local processor and receive release commands from an external source along a neural pathway.

Power could be delivered to an implanted device by a long-life battery [21], although this would have to be replaced at regular intervals, requiring repeated surgical intervention. The alternative is to use some form of energy harvesting to power the implant directly or to recharge a battery. Ultrasound energy harvesting operates at shallow skin depths and will not penetrate through the bone of the skull. It is possible to power implants wirelessly with (i) near-field short-range EM inductive resonant coupling using coiled antennas at frequencies up to 20 MHz, (ii) mid-field coupling (900 MHz) or (iii) far-field (2.5 GHz) EM powering [22]. The use of EM power harvesting is subject to technical constraints to meet recommended safety levels and prevent tissue damage through excessive heating [23]. The specific absorption rate *(SAR)* describes the quantity of EM power that can be absorbed by a tissue and is defined as:

$$SAR = \frac{\sigma E^2}{\rho}. \tag{1}$$

The conductivity of the tissue is σ, the density is ρ and the electric field strength is E. The SAR value is expressed in Watts per kilogram and is averaged over 1 g or 10 g of tissue. In the US the exposure limits for an unrestricted environment, set by the FCC, are 4W/kg for 10g of tissue in the extremities (hands, wrists, feet, ankles) and 1.6 W/kg for 1 g of head, neck and trunk tissue. In other jurisdictions the equivalent ICNIRP and IEEE guidelines specify 2 W/kg for 10 g of head, neck and trunk tissue and 4 W/kg for 10 g of any other limbs [24]. The SAR limits can be converted to power intensities at different frequency ranges and a typical value is 2 W/m^2 for up to 200 MHz and 10 W/m^2 for frequencies greater than 200 MHz [24]. Powering by EM would also require the wearing of an external powering source if true mobility was required. Ideally the implanted device should have a long-life biocompatible power harvesting system that would not have the potential to cause tissue damage and would not depend on external modules.

In previous work [25] we modelled the use of ultrasound to provide harvested power for subcutaneous nanowire-based nanodevices. We then extended that work by modelling the use of arrays of coupled nanodevices for selective neural stimulation [26]. The resulting CAPs were modelled as a data communications system (200 bit/s maximum rate) using *on-off keying (OOK)* [27]. Our stimulus and communications system is optimised for nerves that are at a shallow depth, are not shielded by bone and can be readily accessed for device array implantation.

In this paper we model a specific potential application: the use of neural data pulses transmitted along the vagus nerve to communicate with a programmable, multi-reservoir, drug-delivery system in the brain as shown in Fig. 1. The vagus nerve is a cranial nerve extending from the brainstem and branching to thoracic, abdominal and retroperitoneal organs. The normal neuronal signals serve to moderate functions such as heart rate, breathing and rate of digestion. Two main trunks (branches), the left and the right, can be accessed either side of the neck. The left branch of the vagus nerve, where VNS electrodes are normally placed in humans, does not include cardiac branches with motor neurons and so does not cause cardiac side effects. The main side effects are hoarseness, cough or shortness of breath [13], with no interference to normal brain function [14].

The neural stimulus system delivers current pulses (> 0.2mA) comparable to those delivered by FDA-approved vagus nerve stimulation (VNS) systems (0.2 mA to 5 mA). Asynchronous data packets composed of CAPs could deliver instructions to an embedded device using a unidirectional neural transmission system. Detecting neural data pulses requires lower power than receiving wireless EM signals. Unidirectional transmission implies that no acknowledgement or resend messages can be sent in the reverse direction. We, therefore, analyse the use of *forward error correction (FEC)* in the receiver to improve performance. The main contributions of our work are as follows:

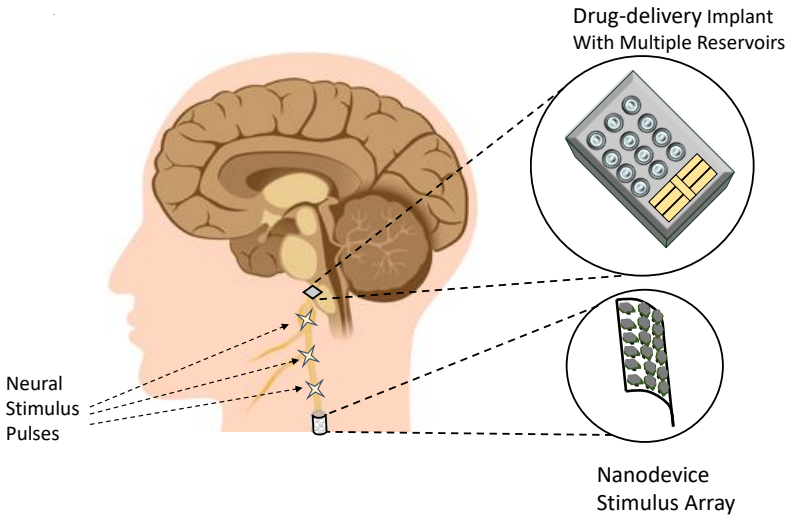

Figure 1: Vagus nerve transmission path delivering data pulses from the stimulus array to the embedded drug-delivery system.

- A model of the generation and propagation of a stimulated neural CAP along the vagus nerve, which shows that it is possible to deliver a maximum OOK data rate of 200 bit/s at ranges between 60 mm and 100 mm;
- An evaluation of the metabolic energy cost of CAP generation in terms of the use of *adenosine triphosphate (ATP)*;
- An analysis of the *bit error rate (BER)* and the *coding gain* using a selection of FEC methods;
- A proposal for simple packet structure for programmable drug-release commands;
- An assessment of the viability of using glucose energy harvesting for powering an implanted drug-delivery system.

This article is organised as follows: the activation of the vagus nerve is described in §2; the data link protocol and error correction in §3; the drug-delivery system components, data packet structure and powering in §4; and our conclusions are presented in §5.

2. Vagus Nerve Stimulation

When a neuron is stimulated, an AP propagates down the neuron's axon to a terminating synapse [12]. The AP cycle duration, typically 5 ms, is called the *Refractory Period (T_{ref})* and a second stimulus applied during this interval will not result in another action potential. The extracellular action potential or *single fibre action potential (SFAP)* is measured on the outside of the neuron with respect to the surrounding extracellular medium. This is smaller in magnitude (on the order of nanovolts) than the underlying intracellular AP. The CAP is the algebraic sum of multiple SFAPs arising from the same external stimulus. The magnitude depends on the number of neurons that are simultaneously activated.

A CAP at a time t and distance l from the stimulating electrode may be expressed as [28]:

$$CAP(t, l) = \sum_{j=1}^{N} \phi_{ej}(t - \tau_j; v_j) \tag{2}$$

where N is the number of active fibres in total in the nerve, ϕ_{ej} is the SFAP of the jth neuron and v_j is the SFAP conduction velocity. The arrival time of the stimulus at the detection point, τ_j is:

$$\tau_j = \frac{l}{v_j} \tag{3}$$

Table 1: Vagus Nerve Axons in Left Branch

Axon Type	*Diameter* (μm)	*Average Number*
Aβ	9-12	825
Aβ, Aδ	3-9	2475
Aδ	1-3	13200

where l is the distance travelled and v_j is the SFAP velocity. The CAP amplitude will reduce with longitudinal distance because the underlying, multi-speed, SFAP bi-phasic peaks will progressively start to cancel each other out [28] giving a reduced summation. This reduction in CAP amplitude with distance is in contrast to the propagation of individual APs, where signal regeneration along the neuron ensures that the amplitude remains constant.

In our model an external source will convert data into coded ultrasound pulses for transmission to an embedded nanodevice array [26]. The array converts the ultrasound into electrical pulses to stimulate bundles of neurons *(fascicles)* in the vagus nerve and create a corresponding stream of modulated CAPs [27]. A receiver implanted at the brainstem must detect these CAPs, record them and then interpret them as instructions using some decoding algorithm.

The level of current needed to artificially stimulate a neuron will depend on the excitability of the neuron, the electrode-neuron distance and the stimulus duration. Larger diameter axons require lower stimulus energy than smaller diameters. Such larger axons have an insulating sheath of *myelin* and are classed as Aα, Aβ, Aδ and B [29]. The myelin sheath has regular gaps at intervals of approximately 2 mm, called *nodes of Ranvier* (typical width of 2 μm), where the AP is regenerated. These nodes are also the points at which an external stimulus pulse will enter the neuron.

The fascicles of the vagus nerve contain both myelinated and unmyelinated axons [30] usually in the proportion of 20% efferent fibers (sending signals from the brain to the body) and 80% afferent (sensory) fibers (carrying information from the body to the brain) [14]. The vast majority are small unmyelinated visceral sensory neurons which carry information from the stomach, intestines, liver, pancreas, and spleen. These are not activated by VNS and would not be activiated by our neural stimulus system. In an adult there can be an average of 16,500 myelinated axons in the left branch and 20,000 in the right branch [31]. The diameter of the myelinated axons varies with 80% less than 3 μm, 15% between 3 μm and 9 μm and 5% greater than 9 μm. The distribution of myelinated axons in the left branch of the vagus nerve, derived in [31], is shown in Table 1. We model a random distribution of 3300 larger diameter axons (3 μm to 12 μm) as input to (2) to generate vagus nerve CAPs as shown in Fig. 2.

The left vagus nerve is located at a depth of 2-3 cm from the side of the neck. This makes it surgically accessible for placing an ultrasound harvesting array and stimulating electrode. At present, electrodes used for VNS are placed at a point on the neck that's equidistant between the clavicle (collar bone) and the base of the skull. This is equivalent to a point half way along the cervical spinal section. In an adult the cervical spinal sections have a total approximate length of 120 mm [32] so our stimulus array will be placed at least 60 mm from the base of the skull and the brain stem (Fig. 1). A stimulus applied at the neck could travel to the brain and be detected by a receiver. In our model we will use a maximum range of 100 mm to allow for physiological variation in the distance from the stimulus array in the neck to the brain stem. Our modelled vagus nerve CAPs are similar in amplitude to therapeutic stimulus CAPs [33]. A typical epilepsy treatment stimulus cycle is 30 s on and 5 minutes off [13] applied continuously throughout the day. The CAP data pulse stream will have a much shorter time span (ms) than VNS and this should help minimise the possibility of side effects.

2.1. Channel Capacity

In our previous work [27] we computed the channel capacity of a typical peripheral nerve (sural nerve) taking into account (i) CAP attenuation with distance, (ii) the ceiling imposed by the neural refractory period of 5 ms and (iii) the background normal neural activity. We now calculate the channel capacity of our modelled vagus nerve and compute the transmission range, subject to these constraints. The CAP attenuation is modelled as a reduction in mean amplitude, $A(z)$, using an empirical exponential function as follows:

$$A(z) = Ge^{-\alpha z}. \tag{4}$$

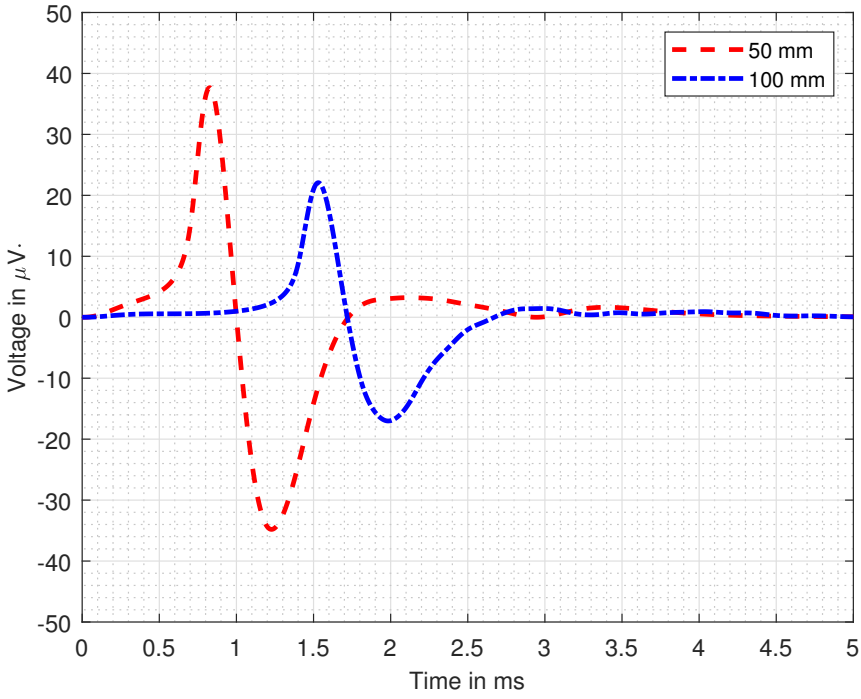

Figure 2: Vagus nerve CAP showing amplitude reduction at two different measuring distances.

The empirical parameters G and α have values that depend on the distribution of axon diameters and the number of activated neurons in the vagus nerve. We assume our multi-neuron path has average white Gaussian noise (*AWGN*) with root mean square (*rms*) values in the range 5 μV to 10 μV [34] [35]. This is in accordance with models for neural noise based on experimental microneurographic measurements of normal (as opposed to stimulated) CAPs [36] [37]. Some models for single neuron AP generation also assume Gaussian noise [38] though others propose the addition of some non-Gaussian frequency-dependent noise [39] to provide more accuracy in single-spike capacity and sorting models. The maximum possible capacity, C bit/s, of a noisy channel with bandwidth U is given by Shannon's formula:

$$C = Ulog_2(1 + SNR). \tag{5}$$

The SNR is the ratio between CAP power and noise power and is derived from the rms noise level, σ_n, and the rms amplitude of the CAP, $A(z)/\sqrt{2}$ (4), as follows:

$$\begin{aligned} SNR(z) &= \frac{A(z)^2}{2{\sigma_n}^2} \\ &= \frac{(Ge^{-\alpha z})^2}{2{\sigma_n}^2}. \end{aligned} \tag{6}$$

The SNR will decrease with distance, because of reduced CAP amplitude, and with higher background noise levels as shown in Fig. 3. The capacity of the vagus nerve can be derived from (5) and (6) using a Nyquist bandwidth of 100 Hz [40]. This bandwidth is based on the maximum pulse rate of 200/s, limited by the refractory period. The capacity ceiling of 200 bit/s can be achieved as long as the SNR is greater than or equal to 3 (equivalent to 4.77 dB). The SNR values at a range of 100 mm are 11 dB (5 μV) and 5 dB (10 μV) so a capacity of 200 bit/s is possible over all noise levels at all ranges up to 100 mm.

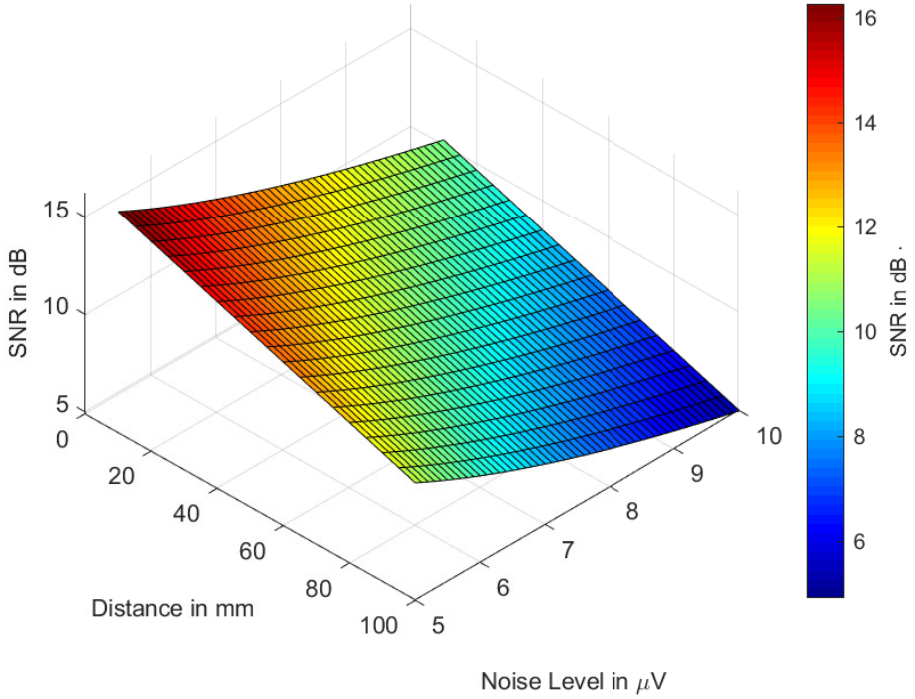

Figure 3: SNR for vagus nerve CAP.

2.2. *Metabolic Energy Requirements*

A conventional EM wireless transmission system can increase the transmission range by increasing the signal power and hence improving the SNR. A wired transmission system can increase the range through the use of regenerators to re-shape and amplify digital signals. Our neural transmission system has elements of both wireless and wired behaviour in that APs are regenerated at each node of Ranvier but the overall CAP is attenuated because of interaction between the APs. The CAP reaches maximum initial amplitude when all larger diameter neurons are activated. A further increase in stimulus energy will trigger lower diameter neurons with slower AP velocities and this will in fact cause greater CAP spreading and a more rapid reduction in amplitude with distance as we showed in previous work [27].

The metabolic energy needed to create the electrical energy of a CAP can be calculated from the amount of ATP that must be hydrolised to support APs. During the transmission of an AP, ATP molecules provide energy to sodium and potassium pumps in the neuron membrane at *every* node of Ranvier to return the neuron to the resting state. The total CAP transmission energy along a specific range in terms of ATP, E_{CAP}, can be calculated as follows:

$$E_{CAP} = \frac{Nl}{g} m E_{AP} \tag{7}$$

where the number of activated neurons is N, the length of the neural transmission path is l, the distance between nodes of Ranvier is g (typically 2 mm), the number of ATP molecules required per AP at each node of Ranvier is m and the energy released per ATP molecule is E_{AP}. The ATP hydrolysis energy is about 30.6 kJ/mol or 5 zJ per molecule [41]. The energy per molecule is often expressed as approximately $12k_BT$ where k_B is Boltzmann's constant and T is the absolute operating temperature. The number of ATP molecules per AP, per node of Ranvier, ranges from 400 to 800×10^6 [42] and we will use an average of 600×10^6 molecules of ATP.

A plot of ATP energy requirements for a vagus nerve CAP against transmission range is shown in Fig. 4. The ATP energy requirement is linear and directly proportional to the transmission range (46 nJ/mm). The plot also shows the decrease in CAP amplitude (voltage) over the same range based on (4). The total number of ATP molecules needed to

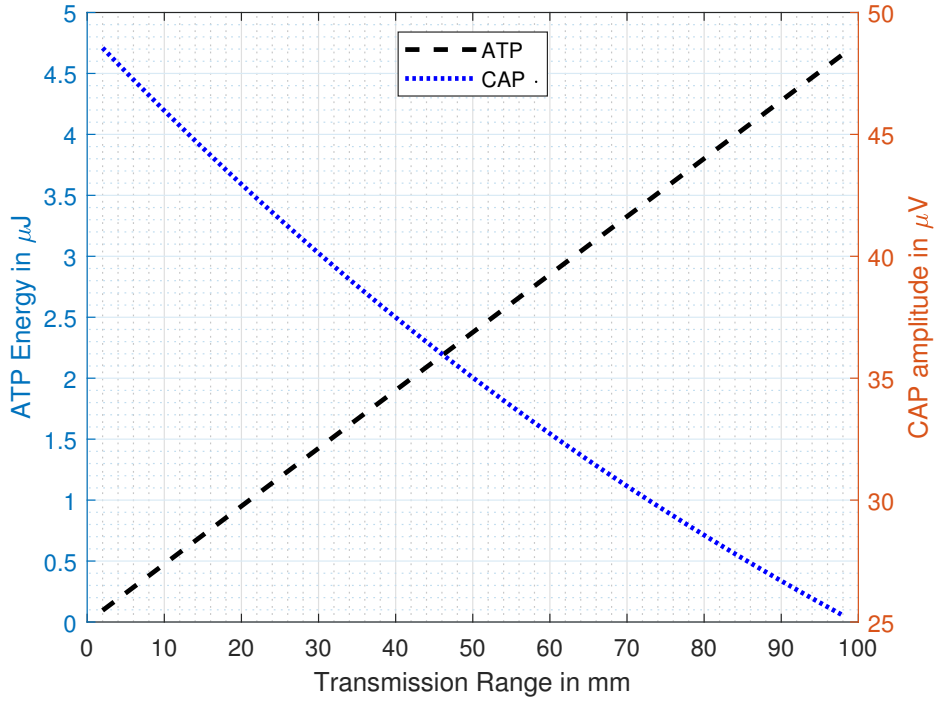

Figure 4: Vagus nerve CAP increase in ATP energy level requirement and decrease in electrical amplitude with distance.

support a CAP for a range of 100 mm is approximately 93×10^{12}. This is a small fraction of the estimated total daily use of 2×10^{26} transient molecules of ATP in the human body [41].

3. Neural Data Link Protocol

The modelled neural CAP communications channel is serial, unidirectional, low bit-rate and therefore suitable for *asynchronous* transmission, where the sender and receiver have separate clocks. Asynchronous data link messages (packets) are of short duration to ensure that the clocks remain closely aligned to each other. A packet usually consists of a start-bit, a character coded as pulses (usually an 8-bit byte) and a stop-bit. Such a packet would have a length of 10 bits and a transmission time of 50 ms with an overhead-to-data ratio of 2/8 or 25%. The send and receive clocks are both based on the expected bit rate and can differ by up to 5% without mis-interpreting the last bit of a ten-bit sequence.

The data packet will deliver instructions to an embedded multi-reservoir drug-delivery system. This can supply repeated doses of either same drug or a selection of different drugs but is likely to be serially activated one reservoir at a time. In our model, a single packet could contain, for example, a two-bit release command and up to six bits of address information (maximum 64 reservoir locations). The number of reservoirs will determine the actual number of addresses so the packet could be shorter than 8 bits if there are fewer than 64 reservoirs. Alternatively, a wide range of stored programmes could be activated using an 8-bit command or smaller, though these would all be pre-set with associated addresses and with no scope for customisation.

3.1. Forward Error Correction

A unidirectional system has no return path for requesting the re-sending of a faulty packet. Error detection and correction, if required, must therefore be provided within the packet and the receiver. An additional parity bit, or check bit, can be used to check that the correct number of "1" values has been received but it can not specify the

Table 2: Error Correction Codes

Code	*Data Bits (max.)*	*Parity Bits*	*Correction Potential (bits)*
Hamming(7 4 3)	4	3	1
Hamming(15 11 3)	11	4	1
BCH(15 7 5)	7	8	2
BCH(15 5 7)	5	10	3
BCH(31 21 5)	21	10	2
Golay(23 12 7)	12	11	3
BCH(31 16 7)	16	15	3

location of, or change, a faulty data value. There are other methods for forward error correction *(FEC)* that can locate and correct faulty bits.

Code repetition is a technique where each bit in a packet of length g bits is sent $n = 2t + 1$ times, $t \geq 1$. The receiver decodes one bit at a time from the group of n into the single value that occurs most often. This will correct up to t errors and will extend the total packet length to $gn + 2$ bits (including the start/stop bits). The transmission time will increase to $(gn + 2)5$ ms, based on a refractory period of 5 ms. Code repetition is simple to implement but the packet length would cause synchronisation challenges between asynchronous transmitter and receiver. Other types of code add fewer extra bits to the packet and these are now discussed.

Block codes add additional parity bits to a byte using a particular algorithm to form a codeword [43]. Decoding and correction is carried out by comparing the received codeword with stored standard generated codewords and finding the closest match. The entire block is decoded at the same time rather than bit-by-bit. Block codes can be classed as *linear* or *cyclical* and include Hamming linear codes, Golay binary code, Bose-Chaudhuri-Hocquenghem *(BCH)* cyclic codes, Reed-Solomon *(RS)* cyclic codes and Turbo Product codes.

Convolutional codes use more complex encoding and decoding methods, using previous bits to encode or decode subsequent bits and hence have memory, unlike block codes that are memoryless. The codes operate on data streams rather than blocks and are more computationally intensive. Our model uses short data packets and we will use examples of block coding on our neural transmission system to study the effect of multiple error detection and correction.

The block code parameters of BCH can be generated from integers $m \geq 3$ and $t < 2^{m-1}$ as follows:

- Codeword length is $n = 2^m - 1$.
- The number of data bits is $k \geq n - mt$ and the number of added parity bits is $n - k \leq mt$.
- The number of errors that can be corrected is t.
- Minimum Hamming distance, $d_{min} \geq 2t + 1$, is a measure of the difference between a received codeword and the closest stored codeword.
- The number of errors that can be detected is $d_{min} - 1$.

Hamming codes are a subset of BCH codes with set values $d_{min} = 3$ and $t = 1$. They can detect two errors and correct one error [44]. Block codes are often expressed in the form (n, k) or (n, k, d_{min}). A Hamming (3,1,2) code is the equivalent of a repetition code with each bit sent three times. Table 2 shows examples of the maximum data payload and correction potential in bits for particular Hamming, Golay and BCH codes. Hamming (7 4 3) and BCH (15 5 7) codes are for the shortest packets (4 and 5 bits respectively) and we will not use these. We are interested in modelling those codes that can be used for a data payload of 7 or 8 bits and can correct 1, 2 or 3 errors. These are Hamming (15 11 3), BCH (15 7 5) and Golay (23 12 7).

3.2. Error Correction Overhead

The more errors an FEC can correct, the greater the cost in additional processing load, longer packets and increased transmission time. With a Hamming (15 11 3) code the minimum number of additional error correction bits for an

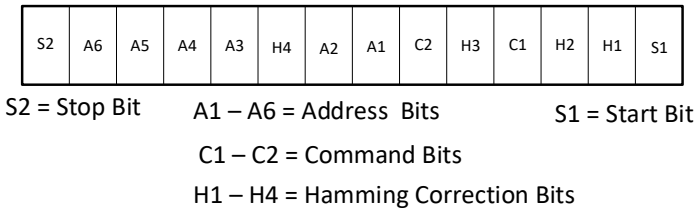

Figure 5: Drug-delivery data packet with command and error correction.

8-bit data message is 4 bits and the total packet length (including start and stop bits) is 14 bits, as shown in Fig. 5. The overhead to data ratio is 6/8 or 75% and the packet will have a transmission time of at least 70 ms. The BCH (15 7 5) and Golay (23 12 7) have overhead to data ratios of 142% and 162.5% with transmission times of 85 ms and 105 ms. The larger overall packet size could increase the probability of a loss of synchronisation between the sender and receiver clocks.

3.3. Coding Gain

The *coding gain* of an FEC is the effective improvement in *bit error rate (BER)* resulting from the use of a particular code on a noisy communications channel. In order to compute the coding gain we must first compute the uncoded BER for CAP transmission along a vagus nerve that has AWGN. The BER measures the probability of data-detection errors occurring as the SNR decreases and is based on the *complementary error function (erfc)* [45], the probability that a "0" is detected instead of a "1" or vice versa. The total probability of bit error for an uncoded OOK stream, BER_{uc}, is calculated by applying the $erfc$ to the derivation of SNR from (6) as follows:

$$\begin{aligned} BER_{uc} &= \frac{1}{2}(erfc)\sqrt{\frac{A(z)^2}{4{\sigma_n}^2}} \\ &= \frac{1}{2}(erfc)\sqrt{\frac{(Ge^{-\alpha z})^2}{4{\sigma_n}^2}}. \end{aligned} \tag{8}$$

The uncoded BER is shown as a surface plot in Fig. 6 across a range of noise levels and a transmission range of 100 mm. The coded BER at the input of the decoder, BER_{id}, is calculated as follows [46]:

$$BER_{id} = \frac{1}{2}(erfc)\sqrt{\frac{k}{n}\frac{(Ge^{-\alpha z})^2}{4{\sigma_n}^2}} \tag{9}$$

where the codeword length is n, the number of data bits is k and the coding rate is k/n. We then use the values of BER_{id} to first calculate the output word error probability, WEP_{od}, as follows:

$$WEP_{od} = \binom{n}{t+1}(BER_{id})^{t+1}(1 - BER_{id})^{n-(t+1)} \tag{10}$$

where the expression $\binom{n}{t+1}$ represents the binomial coefficient. The output coded BER, BER_{od} can then be expressed as:

$$BER_{od} = \frac{d_{min}}{n}(WEP_{od}). \tag{11}$$

The coding gain is a measure of the difference in SNR between uncoded and coded systems for the same BER. The BER is normally plotted against SNR in dB but in our model it can also be plotted against transmission range. The

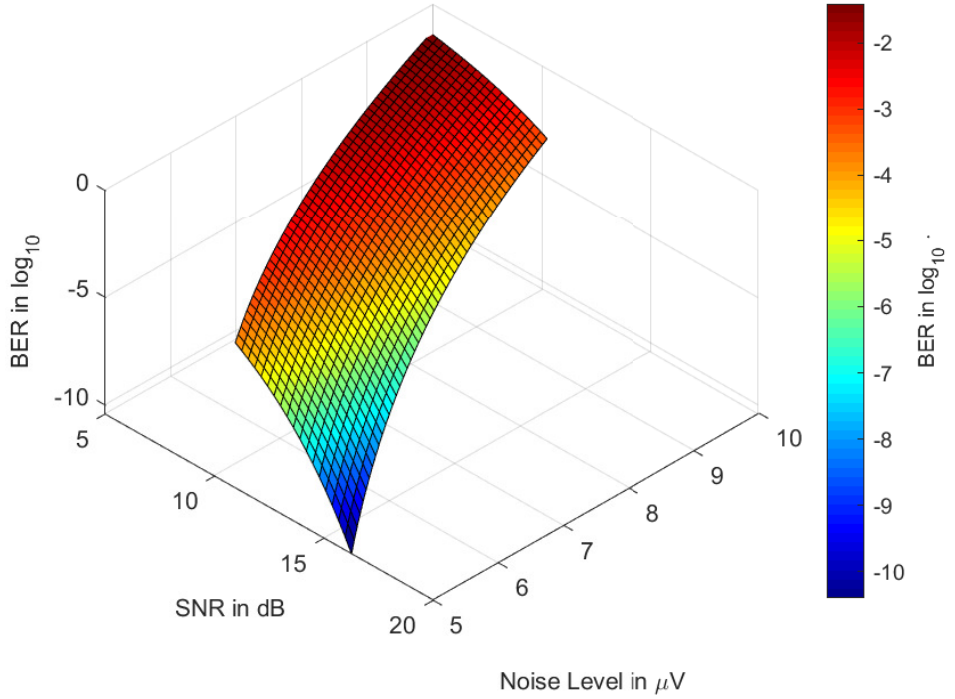

Figure 6: BER for vagus nerve CAP showing increase with noise level and SNR for a transmission range of 100 mm.

Table 3: ATP Code Gain and Parity Bit Cost

BER	*Uncoded mm*	*Gain mm*	*ATP Gain nJ*	*ATP Cost nJ*
10^{-10}	13	20	920	2392
10^{-8}	31	19	874	5704
10^{-6}	56	16	736	10304
10^{-4}	90	13	598	16560

BER plot for our neural transmission system between uncoded data, Hamming (15 11 3), BCH (15 7 5) and Golay (23 12 7) coded data is shown in Fig. 7 for noise levels of 5 μV and 10 μV. The curves show that with FEC (i) a fixed BER can be achieved at a greater range and (ii) a fixed range can have a lower BER.

The plots show that at the lower noise level of 5 μV there is coding gain up to the maximum range of 100 mm. At the higher noise level of 10 μV there is no coding gain after 30 mm range because of the high BER. The Hamming (15 11 3) gain can also be expressed in terms of ATP, calculated from the coding gain in mm. This ATP gain must be offset against the extra ATP needed to carry the corresponding 4 parity bits. Levels of ATP Hamming (15 11 3) gain and the corresponding ATP parity bit cost is shown in Table 3. In every case the ATP cost is greater than the ATP gain, and the difference increases with range. FEC can produce gains and improvements in performance in our neural transmission model but the benefits are sharply reduced with increasing noise level.

4. Drug-delivery System

The embedded drug-delivery system that receives the data packets will have (i) an electrode attached to the vagus nerve near the brain stem to detect the CAP pulse, (ii) an amplification and conversion system to boost the signal

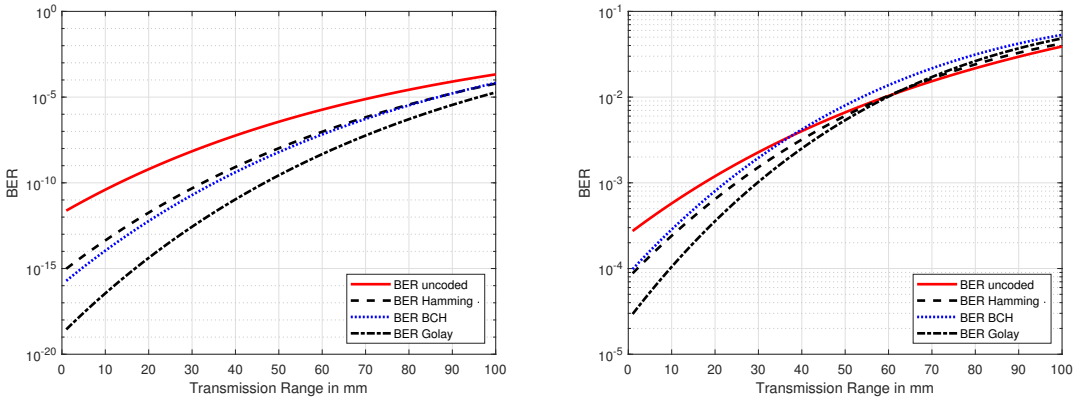

(a) BER and range for 5 μV.

(b) BER and range for 10 μV.

Figure 7: BER plots against transmission range for three different types of FEC and two levels of noise.

power and create a digital bitstream, (iii) a microcontroller unit *(MCU)* to collect and interpret the bitstream, (iv) a drug-delivery mechanism and addressable reservoirs to respond to processor instructions and (v) a power source sufficient to meet all energy demands. The addressable reservoirs could be distributed to different parts of the brain, delivering targetted brain-tumour therapy to locations identified by brain-scans as shown in Fig. 8. A controllable implanted device make it easier to vary different input parameters but the goal is to develop *closed-loop systems* that can record diagnostic requirements and use this as feedback to adjust the drug-delivery instructions.

CAP detection is through a front-end single-channel, single-electrode system similar to those used at present for recording neural activity [47]. The detected pulses will be in the microvolt range. This low voltage is insufficient to switch a transistor directly (with existing CMOS technology) and must be amplified and analysed before it can be designated a logic "1". The detection and amplification function alone places a minimum requirement on the power needed to operate the receiving system, without considering the follow-on drug-delivery functions.

4.1. Detection Electrode and Signal Amplification

The CAP detection electrode must be in close proximity to the transmitting nerve and may be wrapped around it as a cuff electrode. The tripolar nerve cuff electrode design is considered the optimum for low-noise measurement of peripheral nerve activity. Design principles for recording with tripolar cuff electrodes are given by Loeb and Peck [47]. The electrical potentials are differentially measured between a single middle contact and two electrically-shorted symmetrical side contacts. This eliminates any voltage drop (i.e., external noise) that is generated along the inside of the nerve cuff. The length of a tripolar electrode is typically from 15 mm to 30 mm [48].

The cuff electrode must be connected to a low-noise preamplifier to boost the detected CAP signal. The amplified signal can then be sent through filters to a comparator for conversion to logic "1" or "0" using an appropriate sampling rate, and detection threshold set between the noise floor and the expected maximum amplitude. Suitable filters can remove unwanted higher frequency components from the signal as well as having a role in pulse shaping. Single-channel and multi-channel neural amplification and digitalisation is described by Muller et al [49] and their system has a power consumption of 5 μW. Other comparable neural amplifier systems are reviewed in [49] and the power consumption is also in the low microwatt range.

4.2. Microcontroller Unit

The MCU provides the processor functionality to decode the incoming raw bitstream from the comparator and perform any error corrections. The architecture of a comparable MCU is described by Huang et al [50] for an implantable drug-delivery system. This has a *universal asynchronous receiver/transmitter (UART)* to convert serial bits into parallel, a clock input for timing and a decoder to format and forward commands. The power consumption of the MCU and clock generator is 10.68 μW.

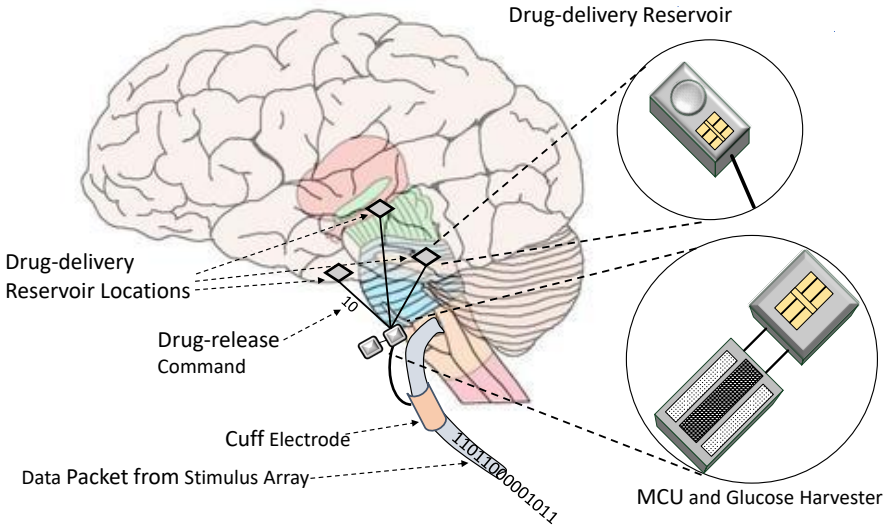

Figure 8: Distributed drug-delivery at multiple locations in the brain.

4.3. Drug-delivery Function

Electrophoretic drug-delivery, as described by Proctor et al [19], applies a voltage difference (typically 1 V) to pump ions from a reservoir across an ion exchange membrane using a *microfluidic ion pump (μFIP)*. The amount of drug delivered depends on the length of time that the voltage is applied. A single type of drug was delivered in trials and the system is being extended for multiple delivery channels that can be singly activated. The operating voltage (1 V) is low and this would indicate a low power requirement.

An alternative method, *electrothermal membrane activation*, was first proposed by Santini et al [20] for multiple drug-delivery. A metallic membrane covering each drug reservoir is heated by an applied electrical current, the membrane ruptures and the drug reservoir then releases its contents. This release model is used by Huang et al[50] in a fabricated delivery system that has a total volume of approximately 30 mm^3.

The power dissipated will depend on the specific materials used in the membrane and the maximum values of current and voltage that can be applied. The activation current in [51] has a nominal value of 1 A and is applied for 10 μs resulting in an activation energy of 25 μJ. A lower activation current with a maximum value of 45 mA is used in [50], applied for 100 ms, results in an activation energy of 6.75 mJ. The power level in both cases would be in the milliwatt range.

4.4. Drug-delivery Activation Commands

The drug-delivery system in[50] has eight addressable reservoirs. Drug release is activated by a ten-bit OOK command that consists of start and stop bits, a five-bit activation key and a three-bit address. The authors state that a more robust forward error correction system would be required in future models.

4.5. Receiver Powering

The electrode, amplification and processor systems will require constant power as they will have to be always-on. The drug delivery function of the implant will have an intermittent and short duration power requirement. Biological energy harvesting could provide a biocompatible and long-life method for delivering the necessary power. A fuel cell using glucose from cerebrospinal fluid circulating around the brain is described by Rapoport et al [52]. The fuel cell has a roughened platinum anode separated from a carbon nanotube cathode by a cation-selective membrane. Glucose is oxidised at the anode while oxygen is reduced to water at the cathode. The authors note that the efficiency of different types of glucose cells varies from 8% to 80%.

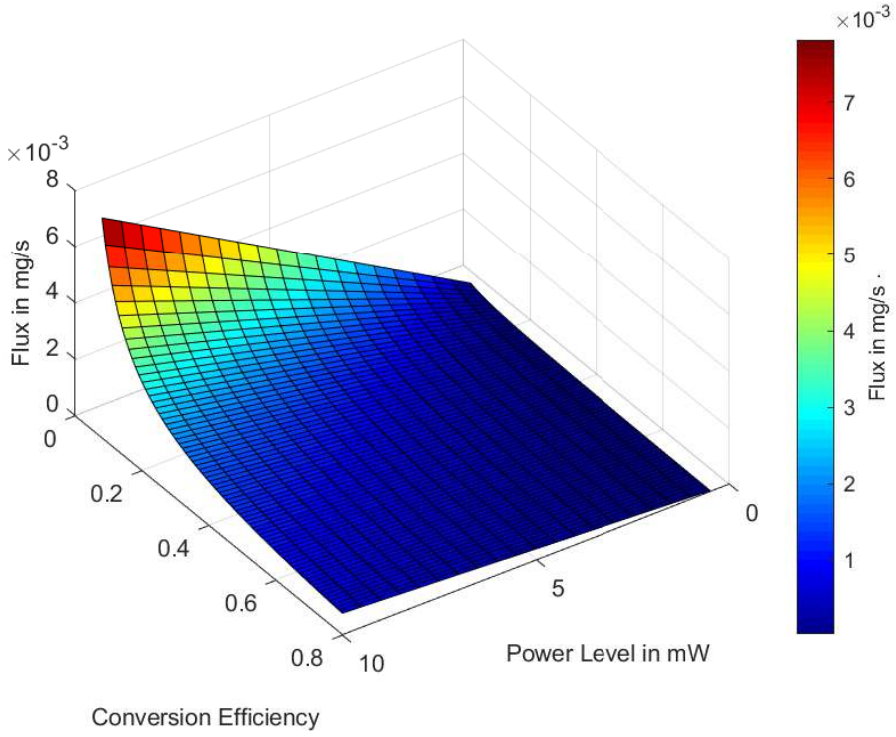

Figure 9: Glucose flux requirement for different power levels at a range of conversion efficiencies.

The glucose flux J_g in milligrams per second (based on 180 mg of glucose per mole) needed to produce a particular power level P is as follows [52]:

$$J_g = \frac{180P}{\eta \Delta G_g} \tag{12}$$

where the conversion efficiency is η and the energy released per mole is $\Delta G_g = 2880$ kJ. The flux of glucose, in milligrams per second, needed to produce a range of power levels at different conversion efficiencies based on (12) is shown in Fig. 9. A power level of 10 mW would require flux levels between .00078 mg/s and .000078 mg/s depending on the efficiency η. The corresponding amount of glucose *per day* needed to produce a continuous power level of 10 mW ranges from 67.5 mg to 675 mg. The daily flow of glucose through the cerebral space is between 250 mg and 440 mg, so the production of higher levels of power could have a major impact on the glucose levels of the cerebrospinal fluid especially at low conversion efficiency levels. The Rapoport fuel cell has power density of .034 μW per mm^2 in a steady state and 1.8 μW per mm^2 in a transient state with an open-circuit voltage of 192 mV.

Improvements in glucose harvesting performance have been demonstrated by Kwon et al [53] who developed a hybrid biofuel cell that uses a metallic cotton fibre cathode and has a power density of 37 μW per mm^2. A dual-source glucose and thermoelectric harvesting system is proposed by Katic et al [54] to improve reliability. The system has a maximum output power of 66 μW. These levels in the microwatt range may be sufficient to power the amplification and MCU components of a drug-delivery system especially if lower-power and lower-voltage electronic technologies emerge, like those described by Theis and Solomon [55]. There would, however, need to be power density into the milliwatt region if drug release using electrothermal membrane activation is to be achieved. Electrophoretic drug delivery might be a more achievable alternative if the voltage level of a glucose powered system could be boosted to 1 V using a step-up converter of the type described by Jayaweera et al [56]. Either way, more efficient glucose harvesting systems would be required if a fully self-powering system is to be realised.

5. Conclusions

Using the vagus nerve for the transmission of digital CAP pulses is an advancement on existing therapeutic neurostimulation. The left branch of the vagus nerve can be accessed at the neck and is at a shallow enough depth to allow ultrasound pulses to penetrate and activate a neural stimulus array. The stimulus pulses travel towards the brainstem and can be intercepted by a receiving electrode and a drug-delivery system. The maximum OOK bit rate of 200 bit/s is constrained by the neural refractory period and the transmission range would typically be between 60 mm and 100 mm

Our unidirectional, asynchronous transmission system would use short packets to maintain synchronisation at both ends. Since there is no return path, there is a need to detect and correct data errors at the receiving end. We modelled the use of block codes for FEC, such as Hamming and BCH, to improve performance. The addition of extra parity bits increases the total packet length, transmission time and ATP consumption. FEC does provide measurable coding gains in our model but these become less significant at greater transmission ranges and lower SNRs (higher noise levels). Simple one-byte (8-bit) commands with additional FEC parity bits can activate an embedded drug-delivery system near the brain. The packet transmission time of tens of milliseconds is an acceptable timeframe in relation to the diffusion and absorption time of a drug in brain tissue.

Existing drug-delivery implants require power in the milliwatt range and voltage levels of 1 V or greater. At present these requirements are met by long-life batteries. Energy harvesting to recharge the battery, using EM systems, has range and safety constraints. We believe that biological energy harvesting using, for example, glucose in the cerebrospinal fluid would be a preferable solution in the longer term. There would need to be major improvements in the power density of the glucose harvesting system and reductions in the power and voltage requirement of the implanted device before such a system would be feasible.

Implanted devices in the future are likely to be deployed at the micro and nano scale with a consequent need for a wider range of non-EM communications systems as described by Akyildiz et al [4]. These nanonetworks of devices will use neural or molecular (chemical) methods of communication within the body and will form part of an *Internet of Things (IoT)* healthcare system as described by Dhanvijay and Patil [57]. CAP data communications along different peripheral nerves could provide an important longer-range transmission option for implant networks, linking clusters of diagnostic and therapeutic nanodevices to gateway points for communicating to and from external processors.

Acknowledgement

This work is supported by the Academy of Finland FiDiPro programme for the project "Nanocommunications Networks" 2012 - 2016, and the Finnish Academy Research Fellow programme under Project no. 284531. It is also partly funded by the Irish Higher Education Authority under the Programme for Research in Third Level Institutions (PRTLI) cycle 5, which is co-funded by the European Regional Development Fund (ERDF), via the Telecommunications Graduate Initiative, and by Science Foundation Ireland via the CONNECT research centre (grant no. 13/RC/2077).

References

[1] R. Ritter, J. Handwerker, T. Liu, M. Ortmanns, Telemetry for implantable medical devices: Part 1 - media properties and standards, IEEE Solid-State Circuits Magazine 6 (2) (2014) 47–51.

[2] R. Sarpeshkar, W. Wattanapanitch, S. K. Arfin, B. I. Rapoport, S. Mandal, M. W. Baker, M. S. Fee, S. Musallam, R. A. Andersen, Low-power circuits for brainmachine interfaces, IEEE Transactions on Biomedical Circuits and Systems 2 (3) (2008) 173–183.

[3] C. Camara, P. Peris-Lopez, J. E. Tapiador, Security and privacy issues in implantable medical devices: A comprehensive survey, Journal of Biomedical Informatics 55 (2015) 272 – 289.

[4] I. F. Akyildiz, F. Brunetti, C. Blázquez, Nanonetworks: A new communication paradigm, Computer Networks (Elsevier) 52 (12) (2008) 2260–2279.

[5] L. Parcerisa-Giné, I. F. Akyildiz, Molecular communication options for long range nanonetworks, Computer Networks 53 (16) (2009) 2753 – 2766.

[6] D. Malak, O. B. Akan, A communication theoretical analysis of synaptic multiple-access channel in hippocampal-cortical neurons, IEEE Transactions on Communications 61 (6) (2013) 2457–2467. doi:10.1109/TCOMM.2013.042313.120799.

[7] H. Ramezani, O. B. Akan, Information capacity of vesicle release in neuro-spike communication, IEEE Communications Letters 22 (1) (2018) 41–44.

[8] M. Veletić, P. A. Floor, Y. Chahibi, I. Balasingham, On the upper bound of the information capacity in neuronal synapses, IEEE Transactions on Communications 64 (12) (2016) 5025–5036.
[9] N. A. Abbasi, D. Lafci, O. B. Akan, Controlled information transfer through an in vivo nervous system, Scientific Reports 8 (1) (2018) 2298.
[10] A. Khodaei, M. Pierobon, An intra-body linear channel model based on neuronal subthreshold stimulation, in: 2016 IEEE International Conference on Communications (ICC), 2016, pp. 1–7.
[11] A. Khodaei, M. Pierobon, Subthreshold linear modeling of dendritic trees: A computational approach, in: 2016 38th Annual International Conference of the IEEE Engineering in Medicine and Biology Society (EMBC), 2016, pp. 235–238.
[12] J. Malmivuo, R. Plonsey, Bioelectromagnetism - Principles and Applications of Bioelectric and Biomagnetic Fields, Oxford University Press, 1995.
[13] S. Krahl, Vagus nerve stimulation for epilepsy: A review of the peripheral mechanisms., Surgical Neurology International.
[14] R. H. Howland, Vagus nerve stimulation, Current Behavioral Neuroscience Reports 1 (2).
[15] F. A. Koopman, S. S. Chavan, S. Miljko, S. Grazio, S. Sokolovic, P. R. Schuurman, A. D. Mehta, Y. A. Levine, M. Faltys, R. Zitnik, K. J. Tracey, P. P. Tak, Vagus nerve stimulation inhibits cytokine production and attenuates disease severity in rheumatoid arthritis, Proceedings of the National Academy of Sciences 113 (29) (2016) 8284–8289.
[16] M. P. Ward, K. Y. Qing, K. J. Otto, R. M. Worth, S. W. M. John, P. P. Irazoqui, A flexible platform for biofeedback-driven control and personalization of electrical nerve stimulation therapy, IEEE Transactions on Neural Systems and Rehabilitation Engineering 23 (3) (2015) 475–484. doi:10.1109/TNSRE.2014.2351271.
[17] X. Dong, Current strategies for brain drug delivery, Theranostics 8 (6).
[18] M. T. Salam, M. Mirzaei, M. S. Ly, D. K. Nguyen, M. Sawan, An implantable closedloop asynchronous drug delivery system for the treatment of refractory epilepsy, IEEE Transactions on Neural Systems and Rehabilitation Engineering 20 (4) (2012) 432–442. doi:10.1109/TNSRE.2012.2189020.
[19] C. M. Proctor, A. Slézia, A. Kaszas, A. Ghestem, I. del Agua, A.-M. Pappa, C. Bernard, A. Williamson, G. G. Malliaras, Electrophoretic drug delivery for seizure control, Science Advances 4 (8).
[20] J. T. Santini Jr, M. J. Cima, R. Langer, A controlled-release microchip, Nature 397.
[21] D. C. Bock, A. C. Marschilok, K. J. Takeuchi, E. S. Takeuchi, Batteries used to power implantable biomedical devices, Electrochimica Acta 84 (2012) 155 – 164. doi:https://doi.org/10.1016/j.electacta.2012.03.057.
[22] R. Jegadeesan, S. Nag, K. Agarwal, N. V. Thakor, Y. Guo, Enabling wireless powering and telemetry for peripheral nerve implants, IEEE Journal of Biomedical and Health Informatics 19 (3) (2015) 958–970. doi:10.1109/JBHI.2015.2424985.
[23] J. Rabaey, M. Mark, D. Chen, C. Sutardja, C. Tang, S. Gowda, M. Wagner, D. Werthimer, Powering and communicating with mm-size implants, in: Design, Automation Test in Europe Conference Exhibition (DATE), 2011, 2011, pp. 1–6. doi:10.1109/DATE.2011.5763123.
[24] Ieee standard for safety levels with respect to human exposure to electric, magnetic, and electromagnetic fields, 0 hz to 300 ghz, IEEE Std C95.1-2019 (Revision of IEEE Std C95.1-2005/ Incorporates IEEE Std C95.1-2019/Cor 1-2019) (2019) 1–312doi:10.1109/IEEESTD.2019.8859679.
[25] M. Donohoe, S. Balasubramaniam, B. Jennings, J. M. Jornet, Powering in-body nanosensors with ultrasounds, IEEE Transactions on Nanotechnology 15 (2) (2016) 151–154. doi:10.1109/TNANO.2015.2509029.
[26] M. Donohoe, B. Jennings, J. M. Jornet, S. Balasubramaniam, Nanodevice arrays for peripheral nerve fascicle activation using ultrasound energy-harvesting, IEEE Transactions on Nanotechnology 16 (6) (2017) 919–930. doi:10.1109/TNANO.2017.2723658.
[27] M. Donohoe, B. Jennings, S. Balasubramaniam, Capacity analysis of a peripheral nerve using modulated compound action potential pulses, IEEE Transactions on Communications 67 (1) (2019) 154–164. doi:10.1109/TCOMM.2018.2871121.
[28] R. S. Wijesinghe, F. L. H. Gielen, J. P. Wikswo, A model for compound action potentials and currents in a nerve bundle i: The forward calculation, Annals of Biomedical Engineering 19 (1) (1991) 43–72. doi:10.1007/BF02368460.
[29] M. D. Mann, The Nervous System in Action, http://michaeldmann.net/The Nervous System In Action.html, 2018.
[30] P. M. Pereyra, W. Zhang, M. Schmidt, L. E. Becker, Development of myelinated and unmyelinated fibers of human vagus nerve during the first year of life, Journal of the Neurological Sciences 110 (1) (1992) 107 – 113.
[31] H. N. Schnitzlein, L. C. Rowe, H. H. Hoffman, The myelinated component of the vagus nerves in man, The Anatomical Record 131 (4) (1958) 649–667.
[32] I. Busscher, J. J. Ploegmakers, G. J. Verkerke, A. G. Veldhuizen, Comparative anatomical dimensions of the complete human and porcine spine., European Spine Journal 19 (7).
[33] M. S. Evans, S. Verma-Ahuja, D. K. Naritoku, J. A. Espinosa, Intraoperative human vagus nerve compound action potentials, Acta Neurologica Scandinavica 110 (4) (2004) 232–238. doi:10.1111/j.1600-0404.2004.00309.x.
[34] K. Guillory, R. Normann, A 100-channel system for real time detection and storage of extracellular spike waveforms, Journal of Neuroscience Methods 91 (1) (1999) 21 – 29. doi:https://doi.org/10.1016/S0165-0270(99)00076-X.
[35] R. R. Harrison, A low-power integrated circuit for adaptive detection of action potentials in noisy signals, in: Proceedings of the 25th Annual International Conference of the IEEE Engineering in Medicine and Biology Society (IEEE Cat. No.03CH37439), Vol. 4, 2003, pp. 3325–3328 Vol.4.
[36] M. Lewicki, Bayesian modeling and classification of neural signals, Neural Computation 6 (1993) 1005–1030.
[37] A. Diedrich, W. Charoensuk, R. J. Brychta, A. C. Ertl, R. Shiavi, Analysis of raw microneurographic recordings based on wavelet de-noising technique and classification algorithm: wavelet analysis in microneurography, IEEE Transactions on Biomedical Engineering 50 (1) (2003) 41–50. doi:10.1109/TBME.2002.807323.
[38] E. Balevi, O. B. Akan, A physical channel model for nanoscale neuro-spike communications, IEEE Transactions on Communications 61 (3) (2013) 1178–1187.
[39] J. Martinez, C. Pedreira, M. J. Ison, R. Q. Quiroga, Realistic simulation of extracellular recordings, Journal of Neuroscience Methods 184 (2) (2009) 285 – 293.
[40] R. L. Freeman, Bits, symbols, bauds, and bandwidth, IEEE Communications Magazine 36 (4) (1998) 96–99. doi:10.1109/35.667424.
[41] L. A. Cole, Chapter 10 - adenosine triphosphate energetics, in: L. A. Cole (Ed.), Biology of Life, Academic Press, 2016, pp. 65 – 77.

[42] S. Hallermann, C. P. J. de Kock, G. J. Stuart, M. H. P. Kole, State and location dependence of action potential metabolic cost in cortical pyramidal neurons, Nature Neuroscience 15 (7).
[43] F. MacWilliams, N. Sloane, The Theory of Error-correcting Codes, Vol. 16, North Holland Mathematical Library, 1977.
[44] A. Ahmadpour, A. A. Sha, M. Ziabari, A novel formulation of hamming code, in: 2009 6th International Conference on Electrical Engineering/Electronics, Computer, Telecommunications and Information Technology, Vol. 02, 2009, pp. 808–811.
[45] L. J. Ippolito, Appendix B: Error Functions and Bit Error Rate, John Wiley & Sons, Ltd, 2008, pp. 363–366.
[46] A. Goldsmith, Coding for Wireless Channels, Cambridge University Press, 2005, Ch. 8, pp. 228–283.
[47] G. Loeb, R. Peck, Cuff electrodes for chronic stimulation and recording of peripheral nerve activity, Journal of Neuroscience Methods 64 (1) (1996) 95 – 103.
[48] L. N. S. Andreasen, J. J. Struijk, Signal strength versus cuff length in nerve cuff electrode recordings, IEEE Transactions on Biomedical Engineering 49 (9) (2002) 1045–1050. doi:10.1109/TBME.2002.800785.
[49] R. Muller, S. Gambini, J. M. Rabaey, A 0.013mm^2, 5μW, DC-coupled neural signal acquisition IC with 0.5 v supply, IEEE Journal of Solid-State Circuits 47 (1) (2012) 232–243. doi:10.1109/JSSC.2011.2163552.
[50] Y.-J. Huang, H.-H. Liao, P.-L. Huang, T. Wang, Y.-J. Yang, Y.-H. Wang, S.-S. Lu, An implantable release-on-demand cmos drug delivery soc using electrothermal activation technique, J. Emerg. Technol. Comput. Syst. 8 (2) (2012) 12:1–12:22. doi:10.1145/2180878.2180884.
[51] J. M. Maloney, S. A. Uhland, B. F. Polito, N. F. Sheppard, C. M. Pelta, J. T. Santini, Electrothermally activated microchips for implantable drug delivery and biosensing, Journal of Controlled Release 109 (1) (2005) 244 – 255, proceedings of the Twelfth International Symposium on Recent Advances in Drug Delivery Systems.
[52] B. I. Rapoport, J. T. Kedzierski, R. Sarpeshkar, A glucose fuel cell for implantable brainmachine interfaces, PLOS ONE 7 (6) (2012) 1–14.
[53] C. H. Kwon, Y. Ko, D. Shin, M. Kwon, J. Park, W. K. Bae, S. W. Lee, J. Cho, High-power hybrid biofuel cells using layer-by-layer assembled glucose oxidase-coated metallic cotton fibers, Nature Communications 9 (1).
[54] J. Katic, S. Rodriguez, A. Rusu, A high-efficiency energy harvesting interface for implanted biofuel cell and thermal harvesters, IEEE Transactions on Power Electronics 33 (5) (2018) 4125–4134. doi:10.1109/TPEL.2017.2712668.
[55] T. N. Theis, P. M. Solomon, In quest of the next switch: Prospects for greatly reduced power dissipation in a successor to the silicon field-effect transistor, Proceedings of the IEEE 98 (12) (2010) 2005–2014. doi:10.1109/JPROC.2010.2066531.
[56] H. M. P. C. Jayaweera, W. P. M. R. Pathirana, A. Muhtaroğlu, Fully integrated ultra-low voltage step-up converter with voltage doubling LC-tank for energy harvesting applications, Journal of Physics: Conference Series 660 (2015) 012017.
[57] M. M. Dhanvijay, S. C. Patil, Internet of things: A survey of enabling technologies in healthcare and its applications, Computer Networks 153 (2019) 113 – 131.